ORIGINAL RESEARCH ARTICLE

Environmental Remediation of Malachite Green Dye by Use of SA-g-P(AAc-MA)/TiO2 Nanocomposite

Hayder H. Shubbar¹, Khudhair M. Mahdi², Khamael abdulsalam Abdul halwas^{3*}, Layth S. Jasim⁴, Maryam Batool⁵

- ¹ Department of Pathological Analyzes, College of Science, University of AL-Qadisiyah, Al Quadisiya,58002, Iraq
- ² Department of Chemistry, University of Sumer, College of Education, Thi-Qar, 64004, Iraq
- ³ Department of Environment, College of Science, University of AL-Qadisiyah, 58002, Iraq
- ⁴ Department of Chemistry, College of Education, University of Al-Qadisiyah, Diwaniyah, 58002, Iraq
- ⁵ Department of Chemistry, University of Sahiwal, Sahiwal, 57000, Pakistan
- *Corresponding author: Khudhair M. Mahdi; khudhairmohammed937@gmail.com

ABSTRACT

This study involved the use of sodium alginate (SA)-g-poly (acrylic acid (AAc)-maleic acid (MA))/titanium dioxide (SA-g-P(AAc-MA)/TiO₂) nanocomposite. The material undergo synthesis by the method of free radical copolymerization for its application in malachite green (MG) dye removal from water. The analysis of the prepared material was carried out by various analytical methods that revealed the presence of different functional groups on the adsorbent's heterogeneous and porous surface. The findings of study showed that nearly 99.56% of MG dye removal take place when solution pH was 2 within 180 min at room temperature. The maximal capacity of adsorbent for dye removal was observed to be 185.2 mg/g. Overall, the study followed pseudo second kinetic and Freundlich isotherm model. Thermodynamic analysis demonstrated the process was spontaneous ($\Delta G = -13.233 \text{ kJ/mol}$) and endothermic ($\Delta H = 27.088 \text{ kJ/mol}$). These results of study showed effectiveness of nanocomposite for dye adsorption from water.

Keywords: Malachite green dye; hydrogel; titanium dioxide; nanocomposite; adsorption; water treatment

ARTICLE INFO

Received: 10 October 2025 Accepted: 31 October 2025 Available online: 11 November 2025

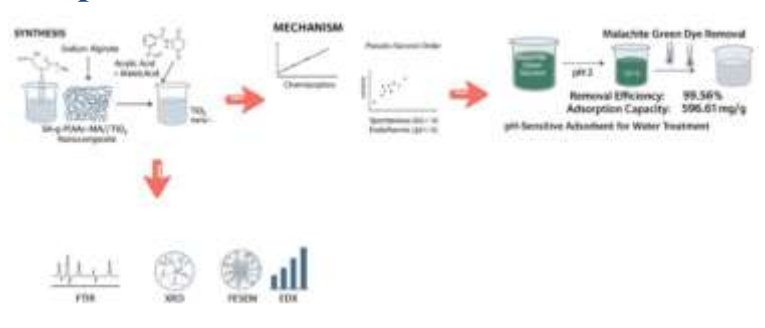
COPYRIGHT

Copyright © 2025 by author(s). Applied Chemical Engineering is published by Arts and Science Press Pte. Ltd. This work is licensed under the Creative Commons Attribution-NonCommercial 4.0 International License (CC BY 4.0). https://creativecommons.org/licenses/by/4.0/

Highlights

- 1. SA-g-P(AAc-MA)/TiO₂ nanocomposite resulted in 99.56% removal of MG dye in 180 minutes
 - 2. Maximum adsorption capacity obtained was 185.2 mg/g
- 3. Adsorption followed pseudo-second and Freundlich models indicating chemisorption on a heterogeneous surface
 - 4. Process was spontaneous and endothermic in nature

Graphical Abstract



1. Introduction

In modern days, dyes (from various industries) are widely discharged to water system without any proper treatment resulting in disturbing the overall environment and water system [1]. These coloring agents are highly toxic, carcinogenic and are hard to remove from water system due to their complex structure [2,3]. Among all dyes, one of the commonly used dyes is malachite green (MG) dye that is well known due to its highly toxic effects [4]. This dye when present in water, causes severe health issue to aquatic organisms and affects the growth of aquatic plants [5]. Researchers are working on the effective removal of this dye from water and for this reason, many methods have been developed till date [6]. The dye removal process include coagulation, adsorption [7], biological process, filtration etc [8-10]. However, these approaches frequently present limitations, including elevated operational costs, secondary pollutant generation, incomplete removal, and diminished efficiency, particularly at low dye concentrations [2,11]. Conversely, adsorption has emerged as a highly promising technique due to its operational simplicity [12,13], cost-effectiveness, adaptable design, and superior removal efficiency, even at trace concentrations [14].

Adsorption process effectiveness depends critically on the physicochemical properties of the adsorbent material ^[15,16]. Recent studies put more emphasis on using polymeric materials like ^[17-21] sodium alginate (SA) as an adsorbent due to presence of the ionic functionalities in it ^[22,23]. The adsorption efficiency of natural polymers can further be enhanced by grafting them with other polymers as acrylic acid (AAc) and maleic acid (MA) ^[24-28]. This yields to synthesis of SA-g-P(AAc-MA), a hydrogel matrix with improved properties. However, the adsorption potential of this matrix can further be tailored by the addition of some semiconductor like titanium dioxide (TiO₂) ^[29,30] that further improved the overall stability ^[31-33] and adsorption characteristics of the resulting material i.e., SA-g-P(AAc-MA)/TiO₂ nanocomposite. This study involved synthesis, characterization and use of SA-g-P(AAc-MA)/TiO₂ nanocomposite for MG dye removal from water. Different kinetic and isothermal models were applied on batch adsorption data in addition to thermal study for better understanding the nature of adsorption.

2. Materials and methods

2.1. Chemicals and reagents

Titanium dioxide nanoparticles (TiO₂), with a purity of \geq 98%, were purchased from Macklin, USA, and used in quantities of 0.1 g. Sodium alginate (SA) (viscosity grade \geq 99%, 0.5 g), acrylic acid (AAc) (inhibitor-free, \geq 99% purity, 4 mL), maleic acid (MA) (\geq 99% purity, 0.5 g), potassium persulfate (KPS) (\geq 99% purity, 0.03 g), and N,N'-methylenebisacrylamide (MBA) (\geq 99% purity, 0.05 g) were all supplied by Himdia, USA. KPS and MBA served as the initiator and crosslinker, respectively, while NaOH and HCl were used to adjust solution pH. Ion-free distilled water was used throughout the synthesis, typically in volumes of 17-20 mL per step.

2.2. Instrumentation

For UV-vis analysis, a Shimadzu UV-1800 spectrophotometer (190-1100 nm), Iran was utilized. For FTIR and Field Emission Scanning Electron Microscopy (FESEM), Shimadzu FTIR 8400S Spectrophotometer (500-4000cm $^{-1}$), Iran, and MIRA3 device, Iran, were employed correspondingly. D₂ Phaser device and 912AB were used for X-ray diffraction (XRD, $2\theta = 10-80^{\circ}$). For shaking, a shaking incubator (LSI-3016A), Lab. Tech, Korea, University of Al Qadisiyah was utilized.

2.3. Preparation of SA-g-P(AAc-MA)/TiO2 nanocomposite

The SA-g-P(AAc-MA)/TiO₂ hydrogel nanocomposite was synthesized using free radical copolymerization in aqueous solution. The process involved dissolving 0.1 g of TiO₂ nanoparticles in 17 mL of ion-free distilled water with continuous stirring for 4 hours, followed by ultrasonication for 4 hours. The

reaction mixture was transferred to a three-neck round-bottom flask equipped with a condenser, separatory funnel, and nitrogen gas inlet within a water bath with continuous stirring until complete dissolution. Subsequently, 0.5 g of sodium alginate (SA) was slowly added to the reaction mixture with stirring, followed by the addition of 4 mL of acrylic acid (AAc). Additionally, 0.5 g of maleic acid (MA), 0.05 g of crosslinking agent (MBA), and 0.03 g of initiator (KPS) dissolved in 1 mL of distilled water were added sequentially through the separatory funnel to the reaction mixture slowly with stirring for 30 minutes at room temperature under nitrogen gas atmosphere. Subsequently, the temperature was raised to 70°C for two hours to complete the polymerization reaction. The resulting SA-g-P(AAc-MA)/TiO₂ nanocomposite hydrogel was immersed in ion-free water to remove unreacted monomers. Finally, it was dried in an electric oven at 50°C to obtain constant weight. The synthesis steps can be illustrated by chemical equations (**Figure 1**) [33,34].

Figure 1. Synthesis of nanocomposite

2.4. Batch adsorption study

The adsorption parameters studied here include time (0-240 min), temperature (5°C to 35°C), adsorbent dose (0.001-0.1 g) as well as pH (2-10) with 20 mL solution volume. The initial and final absorbance values were measured for each experiment fllowed by calculating adsorption capacity (mg/g) and % removal of dye via Equations (1) and (2), correspondingly [35,36]:

$$q_e = \frac{C_o - C_e * V}{m} \tag{1}$$

Removal %=
$$\frac{C_o - C_e}{C_o}$$
 x100 (2)

Where C_0 and C_e = initial and equilibrium dye concentrations correspondingly; m = mass of adsorbent (g), and V = solution volume (L) [35].

3. Results and discussion

3.1. Characterization of adsorbents

3.1.1. Fourier-Transform Infrared Spectroscopy (FTIR)

FTIR of adsorbent before adsorption (**Figure 2**) shows broad absorption band which signifies O–H stretching vibrations and N–H vibrations from crosslinker. Further, C–H stretching vibrations were obtained at 2985 cm⁻¹, while a strong band at 1720 cm⁻¹ indicates C=O stretching vibrations. Also, range 1543-1410 cm⁻¹ represent symmetric and asymmetric vibrations of COO⁻ groups of SA. Bands from 1396 to 1010 cm⁻¹ correspond to O-H, N-H, and C-H groups. The presence of TiO₂ nanoparticles is confirmed by characteristic frequencies at 627 cm⁻¹ (corresponding to Ti-O stretching) and 1404 cm⁻¹ (Ti-O-Ti stretching vibrations), validating TiO₂ incorporation within the SA-g-P(AAc-MA) hydrogel matrix. Following the adsorption of dye, FTIR spectroscopy reveals band shifts toward lower wavelengths, mainly due to H-bonding conforming to effective adsorption [^{33,34,37,38}].

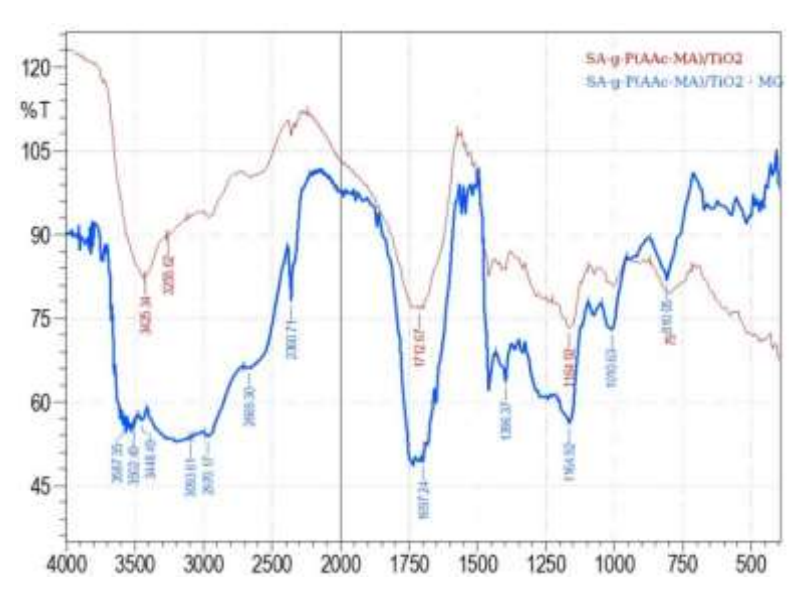


Figure 2. FTIR spectrum of adsorbent before and after adsorption

3.1.2. X-ray Diffraction (XRD)

The XRD pattern (**Figure 3** and **Table 1**) shows broad peak within 2θ (13-30)°, indicating the hydrogel's amorphous nature, with broad band at $2\theta = 21.064^{\circ}$ corresponding to a d-spacing of 4.21771 Å. In contrast, nanocomposite shows distinct crystalline peaks at 25.392°, 36.485°, 48.186°, and 53.685°, revealing TiO_2 nanoparticles. The crystalline size by Debye-Scherrer equation reveal particle sizes 13.61 to 103.35 nm, with the dominant peak at 25.392° corresponding to a crystalline size of 19.79 nm [33,34,37,38].

Table 1. XRD results for nanocomposite.

Peak	2°Theta	θ	d-spacing (A°)	FWHM	Intensity %	D(nm)
1	25.392	12.696	3.507	0.430	100	19.79
2	36.485	18.242	2.462	0.642	46	13.61
3	48.186	24.093	1.888	0.089	40	102.17
4	53.685	26.842	1.707	0.090	22	103.35

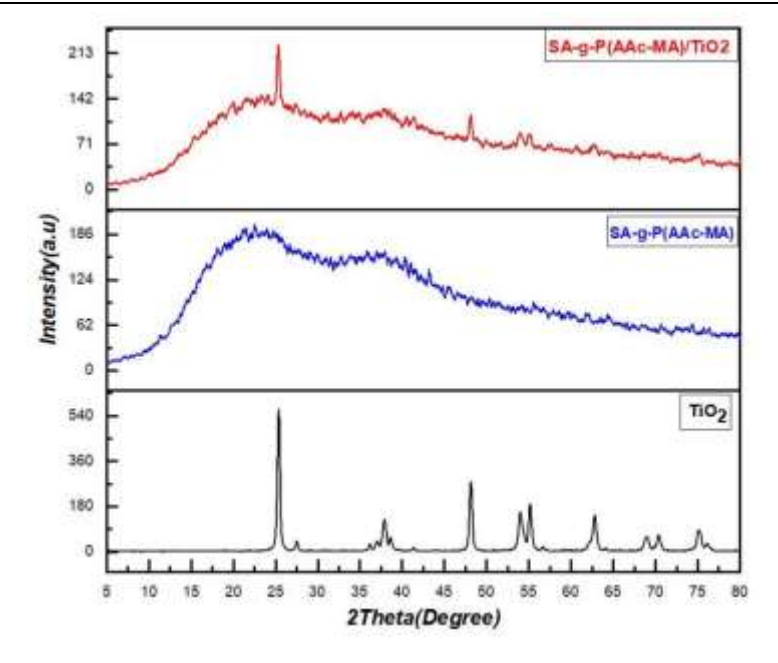


Figure 3. XRD patterns of SA-g-P(AAc-MA) hydrogel and nanocomposite.

3.1.3. Field Emission Scanning Electron Microscopy (FESEM)

FESEM of adsorbent before adsorption shows presence of TiO₂ crystals in anatase phase with uniform sheet-like nanostructures. The surface appears rough and porous, representing a nanocomposite with sponge-like structure and integrated layered network. Further, addition of TiO₂ nanoparticles to hydrogel enhances surface roughness for adsorption (**Figure 4**) [38]. Following adsorption of dye, surface becomes smoother due to filling of pores after adsorption (**Figure 5**) [33,38].

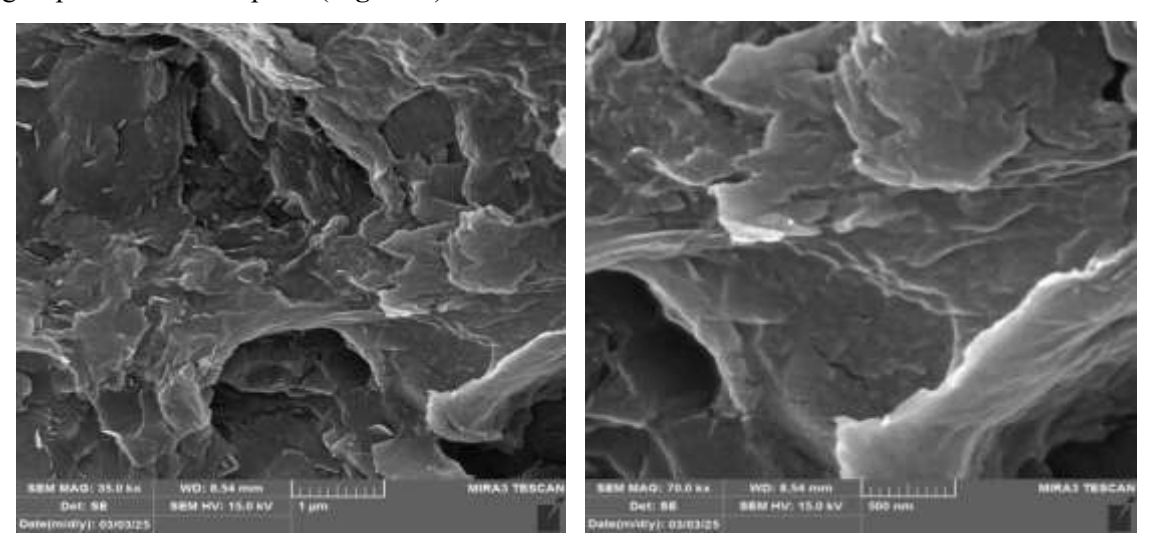


Figure 4. FESEM of nanocomposite before adsorption.

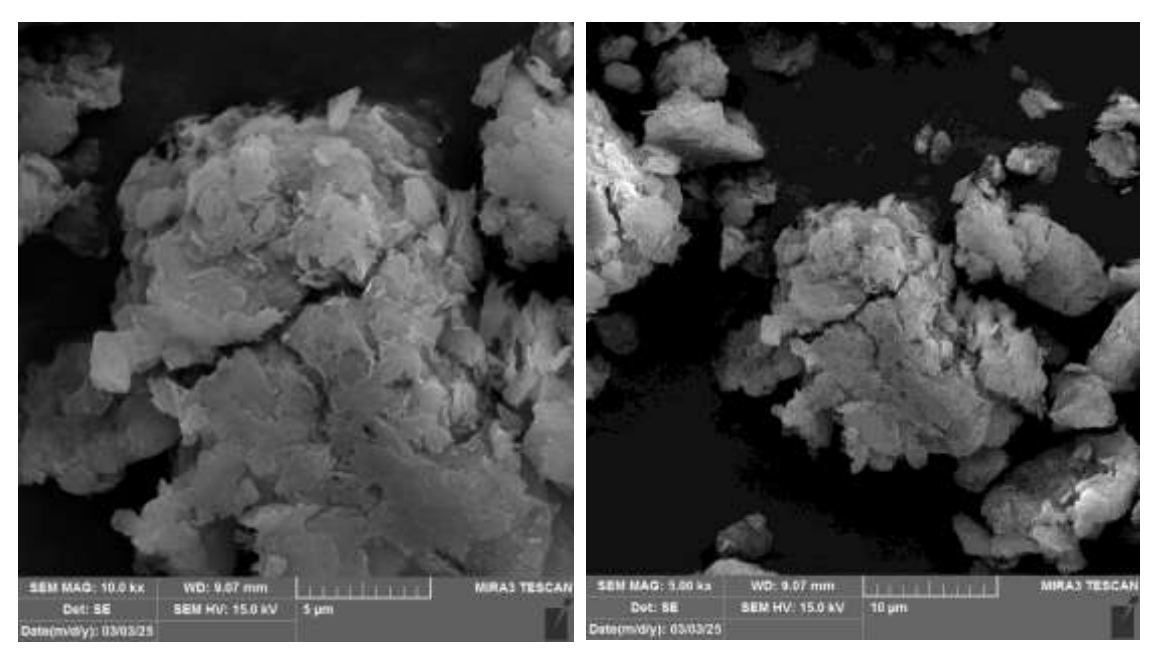


Figure 5. FESEM of nanocomposite after adsorption.

3.1.4. Energy Dispersive X-ray Spectroscopy (EDX)

EDX findings (**Figure 6-7** and **Table 2**) illustrate that oxygen ratio in nanocomposite decreased after adsorption while the carbon ratio increased following dye adsorption. Before adsorption, nanocomposite contained 55.73% carbon, 43.70% oxygen, and 0.58% TiO₂. After adsorption, composition changed to 63.95% carbon, 35.66% oxygen, and 0.38% TiO₂, validating the successful dye uptake [33,39].

		-
Elements %percent	Hydrogel composite before adsorption	Hydrogel composite after adsorption of MG dye
C	55.73	63.95
O	43.70	35.66
Cl	-	-
I	-	-
TiO_2	0.58	0.38

Table 2. Elemental composition of hydrogel nanocomposite before and after adsorption.

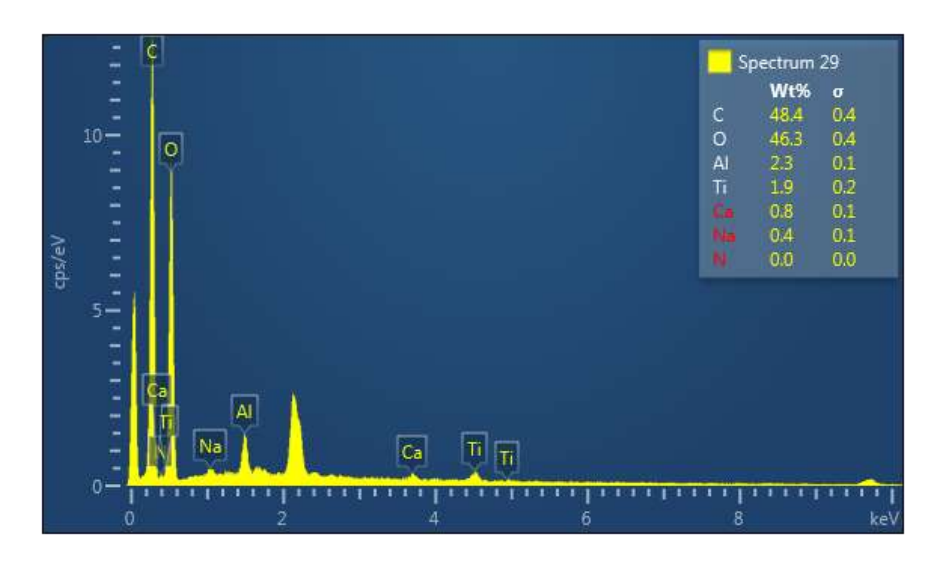


Figure 6. EDX spectrum of SA-g-P(AAc-MA)/TiO2 nanocomposite before adsorption.

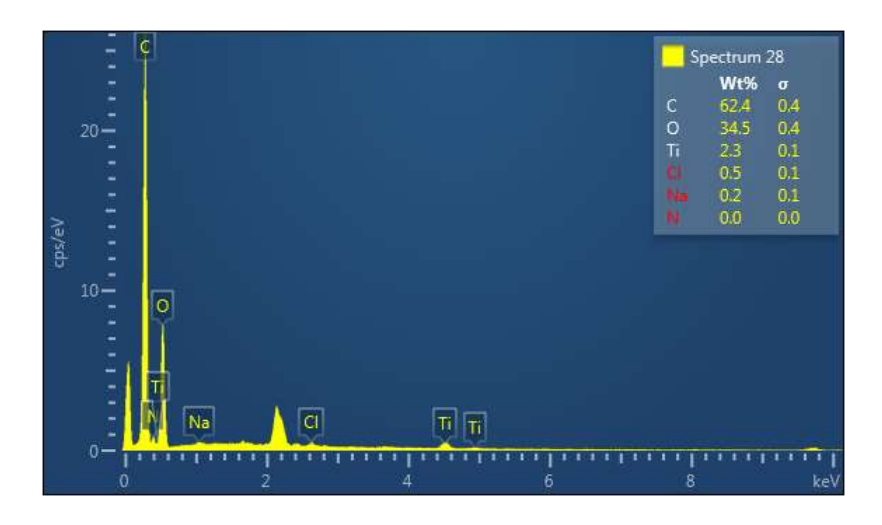


Figure 7. EDX spectrum of nanocomposite after Malachite Green dye adsorption.

3.1.5. Thermogravimetric Analysis (TGA)

The thermal stability of the nanocomposite (**Figure 8**) was evaluated using TGA analysis, where mass changes were measured within the temperature range of 40-900°C at a heating rate of 10°C/min under nitrogen atmosphere. The TGA curve reveals three distinct weight loss stages: the first stage shows a weight loss of 24.99%, attributed to the evaporation of adsorbed water molecules on the surface and removal of moisture trapped within the porous structure of the composite. The second stage exhibits the most significant weight loss of 44.99%, which corresponds to thermal decomposition reactions causing the breaking of chemical bonds in polymer chains and the elimination of oxygen-containing functional groups such as carboxyl and hydroxyl groups in the form of CO₂ and CO, leading to a decrease in the degree of polymerization. The third stage demonstrates a weight loss of 27.98%, attributed to the thermal breakdown of crosslinked polymer chains in the hydrogel nanocomposite and the final decomposition of the carbon skeleton of the composite [31].

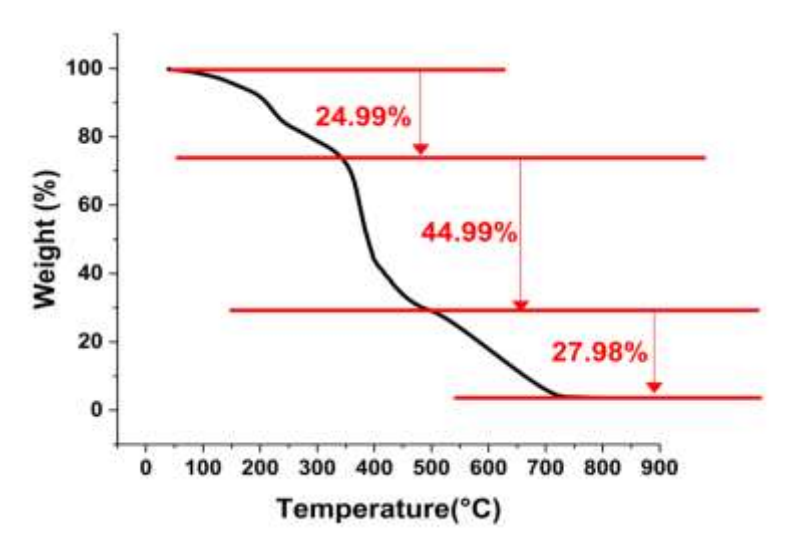


Figure 8. TGA analysis of nanocomposite.

3.1.6. Transmission Electron Microscopy (TEM)

TEM analysis was employed to study the crystalline structure, surface morphology, and particle size distribution. The TEM images of TiO₂ nanoparticles show predominantly spherical particles with clearly visible spherical and heterogeneous structures, indicating that TiO₂ nanoparticles are highly crystalline in nature. The selected area diffraction pattern of the nanoparticles confirms the crystalline nature of the prepared TiO₂ nanoparticles. Particle agglomeration is observed, which is more pronounced in this case. The average

particle size is approximately 19 nm, consistent with the crystalline size obtained from XRD analysis (**Figure 9**) [38].

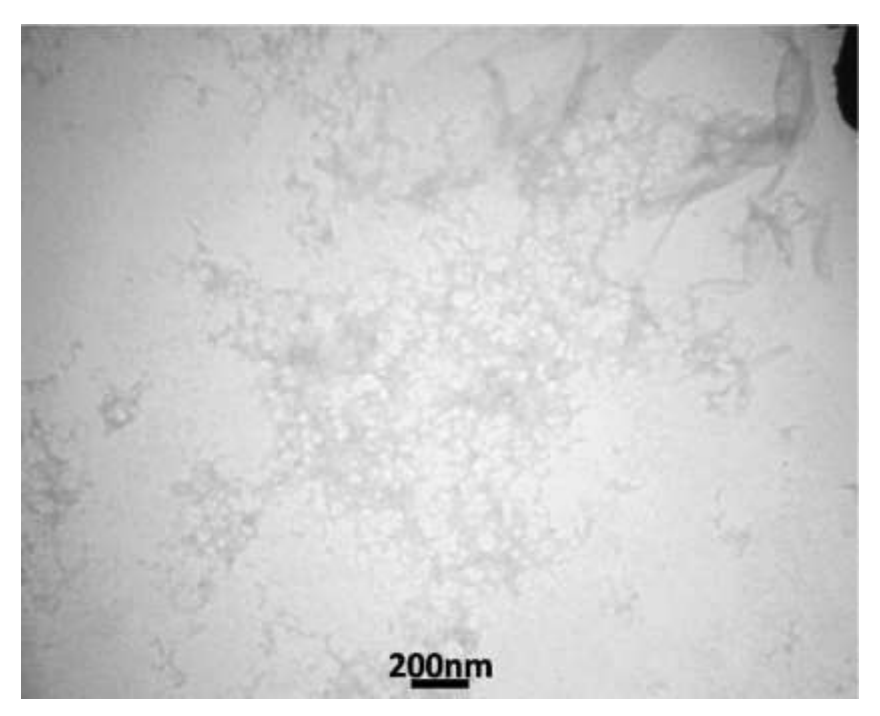


Figure 9. TEM images of nanocomposite before adsorption.

After MG dye adsorption onto surface, TEM images reveal that the spherical shape becomes less distinct due to adsorption by dye molecules. This demonstrates that after MG dye adsorption, the surface becomes smoother and more cohesive due to pore filling by dye molecules, where dye particles completely cover the nanocomposite surface, confirming successful adsorption (**Figure 10**) [38].

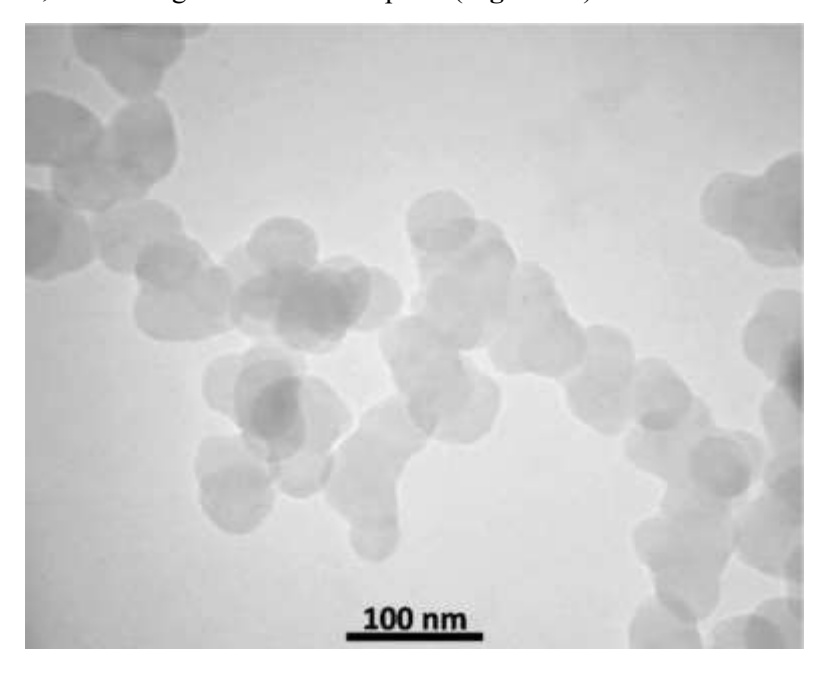


Figure 10. TEM images of nanocomposite after Malachite Green dye adsorption.

3.2. Kinetic study

3.2.1. Adsorbent dose optimization

Adsorbent dose variation effects on Malachite Green dye removal were comprehensively examined across the range 0.001-0.1 g. Removal percentage demonstrated rapid increase from 98.19% to 99.56% with

adsorbent dose elevation from 0.001 g to 0.1 g, subsequently reaching plateau conditions. Conversely, Q_e values exhibited sharp decline with increasing adsorbent dose. At the minimum dose (0.001 g), Q_e achieved peak values, decreasing substantially at higher dosages. This Q_e reduction with increasing adsorbent dose results from available dye molecule saturation in solution and active site overlap phenomena. Optimal adsorbent dose for nanocomposite approximates 0.05 g, achieving dye removal efficiency exceeding 99.5 % (**Figure 11**) [40].

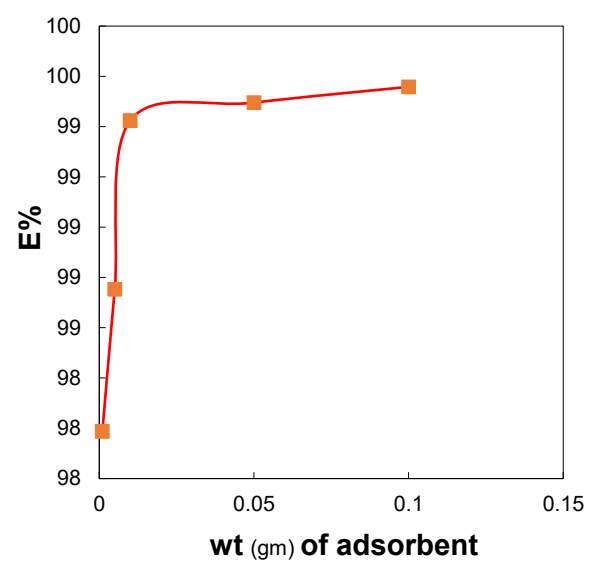


Figure 11. Effect of nanocomposite dose on removal percentage of Malachite Green dye.

3.2.2. Contact time effect and adsorption kinetics

Experimental observations of time study demonstrated a rapid initial adsorption phase occurring within the first 20 minutes, achieving approximately 88.04% removal of Malachite Green dye with a corresponding Q_e of 528.22 mg/g. Following this intensive initial period, particularly after 60 minutes, the adsorption rate progressively decelerated as the system approached equilibrium conditions. At the 180-minute timepoint, the dye removal reached 99.43%, with an associated Q_e of 596.61 mg/g (**Figure 12**) [41].

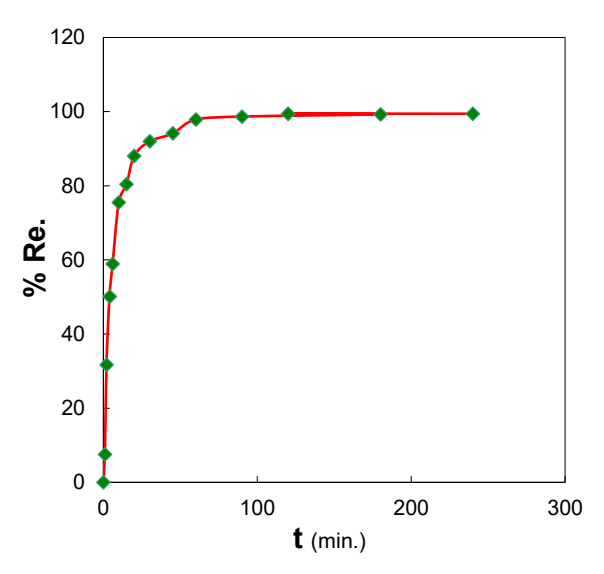


Figure 12. Effect of contact time.

3.2.3. Kinetic modeling analysis

The pseudo-first-order model postulates that the rate of adsorption site occupation correlates directly with the concentration of available. Pseudo-second model proposes that chemisorption constitutes the rate-determining step. The mathematical expressions for these kinetic models are presented in Equations (3) and (4) [41].

$$\log(Q_e - Q_t) = \log Q_e - \frac{k_1}{2.303}t$$
 (3)

$$\frac{t}{Q_{t}} = \frac{1}{k_{2}Q_{e}^{2}} + \frac{t}{Q_{e}} \tag{4}$$

Where q_t and q_e represent the quantities of adsorbate adsorbed (mg/g) at time t and equilibrium, respectively, while k_1 and k_2 denote the pseudo-first-order rate constant (min⁻¹) and pseudo-second-order rate constant (g/mg·min), respectively.

Application of the linearized pseudo-first-order model yielded a slope of $-0.0405 \, \text{min}^{-1}$ and intercept of 5.3841, generating a calculated Q_e value of approximately 242.16 mg/g with a correlation coefficient (R²) of 0.888. The substantial discrepancy between the calculated Q_e (242.16 mg/g) and experimental Q_e (596.61 mg/g) indicates inadequate model fitting to the experimental data. Significantly, pseudo-second model demonstrated exceptional correlation with experimental data (R² = 0.9989), with calculated Q_e closely approximating experimental value. The superior R² value indicates that process follows pseudo-second kinetics, confirming chemisorption (**Figure 13-14** and **Table 3**) [11].

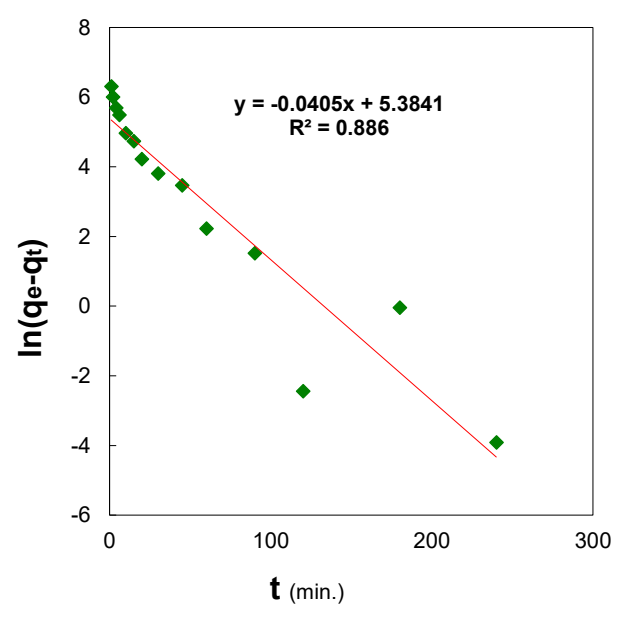


Figure 13. Pseudo-first-order kinetic model plot for Malachite Green dye adsorption.

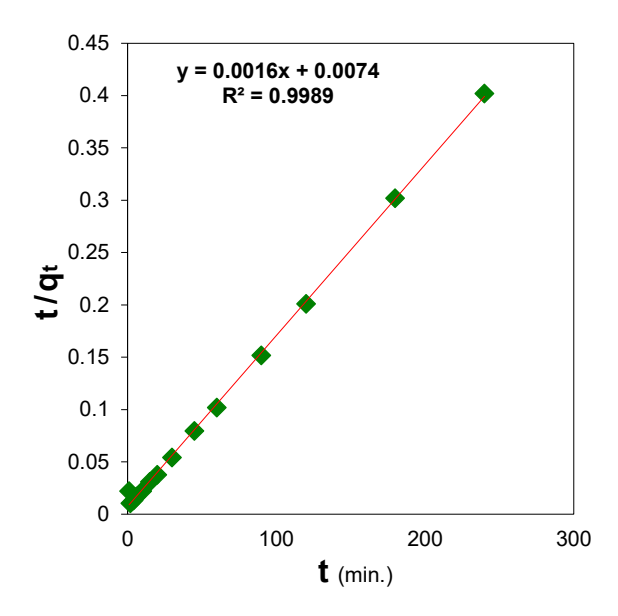


Figure 14. Pseudo-second-order kinetic model plot for Malachite Green dye adsorption.

Table 3. Kinetic model parameters for pseudo-first and pseudo-second models. Experimental Q_e (mg/g) = 596.61 mg/g.

	F	rist Order	•				Second	l Order		
Slope	intercept	\mathbf{k}_1	$\mathbf{q}_{\mathbf{e}}$	\mathbb{R}^2	Slope	intercept	q e	k ₂	h	R ²
-0.040	5.384	0.040	217.913	0.8860	0.002	0.007	625	0.0003	135.135	0.9989

3.3. Thermodynamic and isothermal study

3.3.1. Temperature effect on adsorption

The adsorption behavior of Malachite Green dye onto the SA-g-P(AAc-MA)/TiO₂ nanocomposite was comprehensively examined as a function of initial dye concentration and temperature. The equilibrium adsorption capacity (Q_e) demonstrated direct dependence on both dye concentration and experimental temperature. At any given temperature, increasing dye concentration resulted in an increase in both equilibrium concentration and corresponding Q_e values. A particularly significant finding revealed the substantial temperature influence on adsorption process. Temperature elevation from 5°C to 35°C produced notable Q_e enhancement across all initial dye concentration ranges, definitively establishing endothermic nature of Malachite Green dye adsorption onto SA-g-P(AAc-MA)/TiO₂ nanocomposite (**Figure 15**) [42].

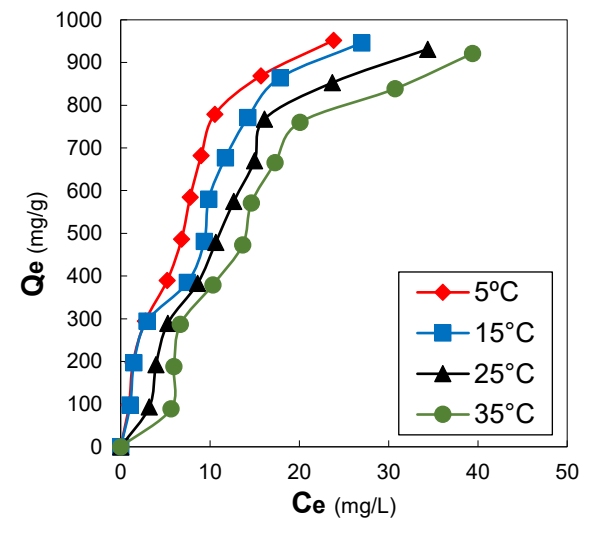


Figure 15. Effect of temperature on adsorption capacity (Qe) of dye by SA-g-P(AAc-MA)/TiO2 nanocomposite.

3.3.2. Thermodynamic parameters

Thermodynamic analysis through Van't Hoff plotting revealed critical process characteristics at 25°C. The positive enthalpy change ($\Delta H = 27.088 \text{ kJ/mol}$) confirms the endothermic nature of the adsorption process, indicating heat absorption from the surrounding environment. The negative Gibbs free energy change ($\Delta G = 13.233 \text{ kJ/mol}$) demonstrates process spontaneity at the investigated temperature. The positive entropy change ($\Delta S = 135.135 \text{ J/K/mol}$) indicates increased randomness or disorder at the solid-liquid interface during adsorption, particularly favoring spontaneity at elevated temperatures (**Figure 16**) [1].

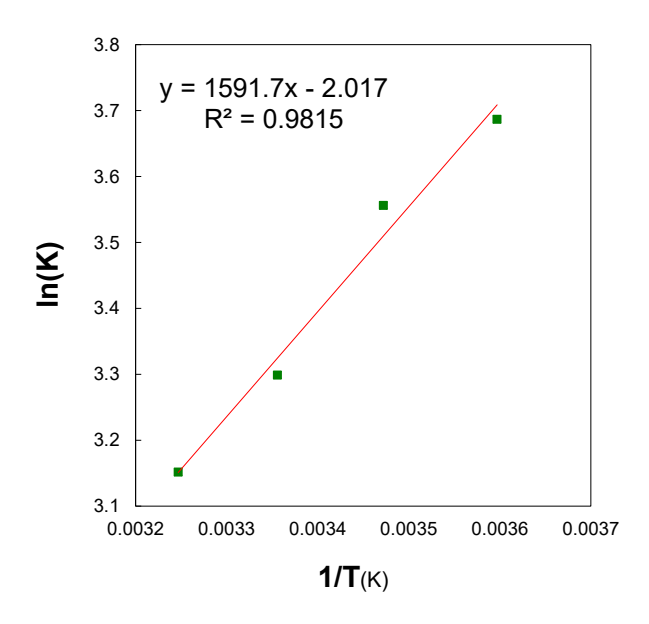


Figure 16. Van't Hoff plot for thermodynamic parameter determination of Malachite Green dye adsorption.

3.3.3. Adsorption isotherm analysis

Equilibrium adsorption data for Malachite Green dye underwent comprehensive evaluation using linearized forms of three established isotherm models: Langmuir, Freundlich, and Temkin. Comparative analysis (**Figure 17-19** and **Table 4**) revealed that Freundlich isotherm model provided superior experimental data representation, indicating multilayer adsorption occurrence on heterogeneous surface sites. The Langmuir model demonstrated reasonable correlation, while the Temkin model exhibited moderate fitting quality. The exceptional Freundlich model correlation suggests heterogeneous surface characteristics with favorable binding conditions facilitate the adsorption process [1].

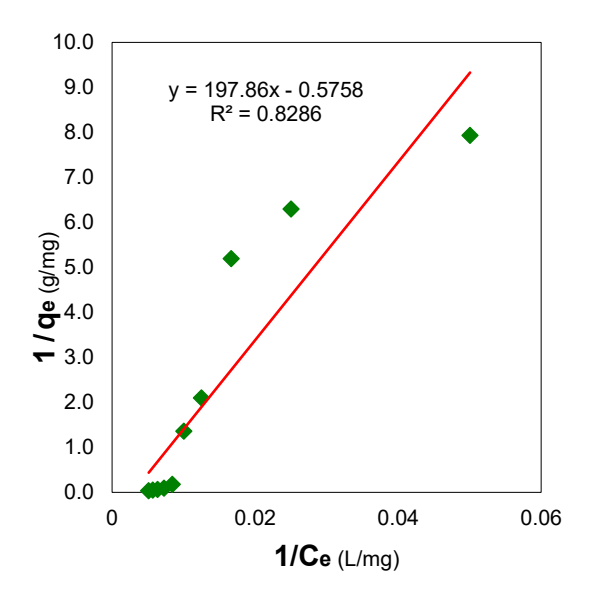


Figure 17. Langmuir isotherm model for dye adsorption.

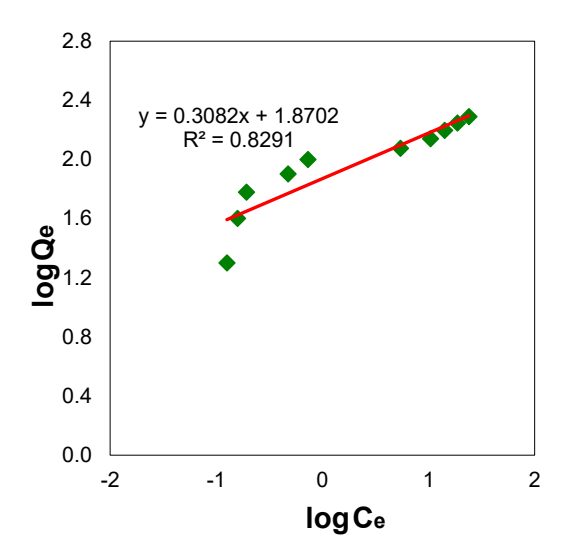


Figure 18. Freundlich isotherm model for dye adsorption.

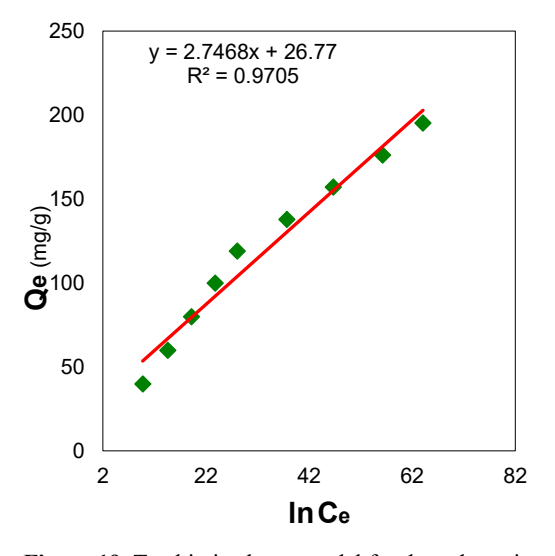


Figure 19. Temkin isotherm model for dye adsorption.

Table 4. Isotherm model parameters for Langmuir, Freundlich, and Temkin models.

Langmuir	Freundlich	Temkin
q ₀ (mg/g): 625	Kf (mg g ⁻¹): 185.2	B (J/mol): 1095.4
b (L/g): 0.0025	1/n: 0.487	AT (L/g): 0.215
R ² : 0.845	R ² : 0.965	R ² : 0.923

3.4. Effect of pH and nanocomposite dose

3.4.1. pH influence on adsorption capacity

The influence of solution pH on Malachite Green dye adsorption capacity was systematically investigated across the pH range 2-10. Maximum adsorption capacity ($Q_e = 596.61 \text{ mg/g}$) was achieved at pH 2. As pH increased from 2 to 10, the Q_e values maintained relative stability until pH 6, followed by gradual decline at higher pH values. These observations result from variable electrostatic interactions between the adsorbent surface and cationic dye molecules under different pH conditions. At acidic pH values (2-4, **Figure 20**), nanocomposite surface undergoes protonation, establishing favorable conditions for cationic Malachite Green dye adsorption through electrostatic attraction complemented by additional interactions including π - π stacking mechanisms [1].

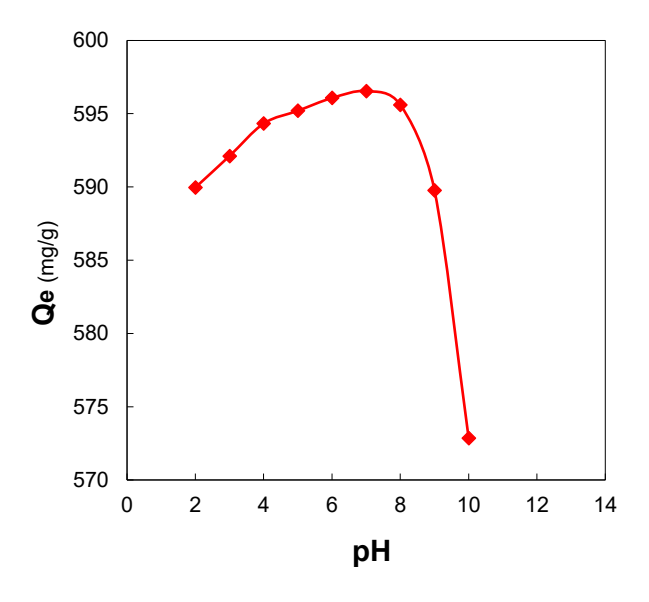


Figure 20. Effect of pH on Qe of dye.

5. Conclusion

In this study, a novel hydrogel nanocomposite SA-g-P(AAc-MA)/TiO₂ was successfully synthesized and analysed by FTIR, XRD, FESEM, and EDX techniques for its use in MG dye removal. Findings of the study showed that 99.56 % (185.2 mg/g) of MG dye removal take place in highly acidic environment. The studied nanocomposite was highly pH-dependent. Overall, the process was chemical adsorption that was confirmed by the fitness of the pseudo-second kinetic model. Furthermore, the heterogeneous nature of the process was revealed by high regression coefficient value of Freundlich model. Thermally, study was both spontaneous and endothermic in nature.

Conflict of interest

The authors declare no conflict of interest.

References

- 1. Muinde VM; Onyari JM; Wamalwa B; Wabomba JN. Adsorption of malachite green dye from aqueous solutions using mesoporous chitosan–zinc oxide composite material. Environmental Chemistry and Ecotoxicology. 2020;2:115-125
- 2. Shah, A.; Arjunan, A.; Manning, G.; Zakharova, J.; Andraulaki, I.; Batool, M. The effect of dose, settling time, shelf life, storage temperature and extractant on Moringa oleifera Lam. protein coagulation efficiency. *Environmental Nanotechnology, Monitoring & Management* **2024**, 21, 100919.
- 3. Zeeshan M; Javed T; Kumari C; Thumma A; Wasim M; Taj MB; Sharma I; Haider MN; Batool M. Investigating the interactions between dyes and porous/composite materials: a comprehensive study. Sustainable Chemistry for the Environment. 2025:100217
- 4. Khattri S; Singh M. Removal of malachite green from dye wastewater using neem sawdust by adsorption. Journal of hazardous materials. 2009;167(1-3):1089-1094
- 5. Garg V; Kumar R; Gupta R. Removal of malachite green dye from aqueous solution by adsorption using agroindustry waste: a case study of Prosopis cineraria. Dyes and pigments. 2004;62(1):1-10
- 6. Garg, V.; Kumar, R.; Gupta, R. <u>Removal of malachite green dye from aqueous solution by adsorption using agroindustry waste: a case study of Prosopis cineraria.</u> *Dyes and pigments* **2004**, 62 (1), 1-10.
- 7. Verma, A.; Thakur, S.; Mamba, G.; Gupta, R. K.; Thakur, P.; Thakur, V. K. <u>Graphite modified sodium alginate hydrogel composite for efficient removal of malachite green dye.</u> *International Journal of Biological Macromolecules* **2020**, 148, 1130-1139
- 8. Bdaiwi, Z. M.; Abbas, G. J.; Ghanem, H. T. <u>Synthesis, Characterization of Heterocyclic Compounds Containing Dapsone</u>. *International Journal of Drug Delivery Technology* **2022**, 12 (3), 1446-1452, Article. DOI: 10.25258/ijddt.12.3.87 Scopus.
- 9. Shah A; Arjunan A; Thumma A; Zakharova J; Bolarinwa T; Devi S; Batool M. Adsorptive removal of arsenic from drinking water using KOH-modified sewage sludge-derived biochar. Cleaner Water. 2024;2:100022
- 10. Chinthalapudi, N.; Kommaraju, V. V. D.; Kannan, M. K.; Nalluri, C. B.; Varanasi, S. <u>Composites of cellulose nanofibers and silver nanoparticles for malachite green dye removal from water.</u> <u>Carbohydrate Polymer Technologies and Applications 2021</u>, 2, 100098
- 11. Urooj H; Javed T; Taj MB; Nouman Haider M. Adsorption of crystal violet dye from wastewater on Phyllanthus emblica fruit (PEF) powder: kinetic and thermodynamic. International Journal of Environmental Analytical Chemistry. 2024;104(19):7474-7499
- 12. Bukhari A; Javed T; Haider MN. Adsorptive exclusion of crystal violet dye from wastewater by using fish scales as an adsorbent. Journal of Dispersion Science and Technology. 2023;44(11):2081-2092
- 13. Imran MS; Javed T; Areej I; Haider MN. Sequestration of crystal violet dye from wastewater using low-cost coconut husk as a potential adsorbent. Water Science and Technology. 2022;85(8):2295-2317
- 14. Javed, T.; Thumma, A.; Uddin, A. N.; Akhter, R.; Babar Taj, M.; Zafar, S.; Mahmood Baig, M.; Shoaib Ahmad Shah, S.; Wasim, M.; Amin Abid, M. <u>Batch adsorption study of Congo Red dye using unmodified Azadirachta indica leaves: isotherms and kinetics. Water Practice & Technology</u> **2024**, 19 (2), 546-566.
- 15. Arshad R; Javed T; Thumma A. Exploring the efficiency of sodium alginate beads and Cedrus deodara sawdust for adsorptive removal of crystal violet dye. Journal of Dispersion Science and Technology. 2024;45(12):2330-2343
- 16. Mittal, A. <u>Adsorption kinetics of removal of a toxic dye, Malachite Green, from wastewater by using hen feathers.</u> *Journal of hazardous materials* **2006**, 133 (1-3), 196-202
- 17. Zhang T; Xiao S; Fan K; He H; Qin Z. Preparation and adsorption properties of green cellulose-based composite aerogel with selective adsorption of methylene blue. Polymer. 2022;258:125320
- 18. Eidan, D. M.; Abdul Halwas, K. A.; Hassan, M. M.; Jasim, l. S.; Tariq, T. B. Role of Nano-Hydrogel Based Materials for Water Purification: A Comprehensive Review. *Journal of Nanostructures* **2025**, 15 (3), 1508-1518. DOI: 10.22052/jns.2025.03.063.
- 19. Bdaiwi ZM; Abbas GJ; Ghanem HT. Synthesis, Characterization of Heterocyclic Compounds Containing Dapsone. International Journal of Drug Delivery Technology. 2022;12(3):1446-1452.10.25258/ijddt.12.3.87
- 20. Bdaiwi ZM; Ghanem HT. Synthesis and characterization of some oxazepine compounds from 2- amino thiazole. Journal of Global Pharma Technology. 2020;12(6):291-303
- 21. Al-Suraify SMT; Hussien LB. Synthesis and characterization of new compounds derived from 1H-indol-5-ylamine. Applied Nanoscience (Switzerland). 2023;13(3):2083-2092.10.1007/s13204-021-02080-3
- 22. Rahmani M; Dadvand Koohi A. Adsorption of malachite green on the modified montmorillonite/xanthan gumsodium alginate hybrid nanocomposite. Polymer Bulletin. 2022;79(10):8241-8267
- 23. Amiri-Hosseini S; Hashempour Y. Photocatalytic removal of Malachite green dye from aqueous solutions by nano-composites containing titanium dioxide: A systematic review. Environmental Health Engineering And Management Journal. 2021;8(4):295-302
- 24. Melhi S; Algamdi M; Alqadami AA; Khan MA; Alosaimi EH. Fabrication of magnetically recyclable nanocomposite as an effective adsorbent for the removal of malachite green from water. Chemical Engineering Research and Design. 2022;177:843-854

- 25. Li, Y.; Sun, J.; Du, Q.; Zhang, L.; Yang, X.; Wu, S.; Xia, Y.; Wang, Z.; Xia, L.; Cao, A. Mechanical and dye adsorption properties of graphene oxide/chitosan composite fibers prepared by wet spinning. *Carbohydrate polymers* **2014**, 102, 755-761.
- 26. Haider, M. N. Enhanced degradation of reactive violet 1 (RV1) dye using gamma and UV irradiation Coupled with hydrogen peroxide. *Radiation Physics and Chemistry* **2025**, 113191.
- 27. Abdulsahib WK; Sahib HH; Mahdi MA; Jasim LS. Adsorption Study of Cephalexin Monohydrate Drug in Solution on Poly (vinyl pyrrolidone-acryl amide) Hydrogel Surface. International Journal of Drug Delivery Technology. 2021;11(4):1169-1172.10.25258/ijddt.11.4.9
- 28. Ganduh SH; Aljeboree AM; Mahdi MA; Jasim LS. Spectrophotometric Determination of Metoclopramide-HCL in the Standard Raw and it Compared with Pharmaceuticals. Journal of Pharmaceutical Negative Results. 2021;12(2):44-48.10.47750/pnr.2021.12.02.008
- 29. Naeem R; Shakir S; Sharif S; Afzal S; Bashir S; Mansoor MA. The photoelectrochemically enhanced oxygen evolution reaction via thin films of novel (1: 2: 1) SnO-Mn2O3-TiO2 hybrid nanotubes. Surfaces and Interfaces. 2024;46:104034
- 30. Naeem R; Ehsan MA; Yahya R; Sohail M; Khaledi H; Mazhar M. Fabrication of pristine Mn 2 O 3 and Ag–Mn 2 O 3 composite thin films by AACVD for photoelectrochemical water splitting. Dalton Transactions. 2016;45(38):14928-14939
- 31. Hussain S; Salman M; Al-Ahmary KM; Ahmed M. Synthesis of potential adsorbent for removal of malachite green dye using alginate hydrogel nanocomposites. International Journal of Biological Macromolecules. 2025;289:138816
- 32. Al-Hasan, H. A.; Munadi Th. Al-Suraify, S.; Othman, M. A. M.; Jasim, L. S.; Batool, M. <u>Activated Nano-Carbon from Natural Sources for Water Treatment: A Comprehensive Review.</u> *Journal of Nanostructures* **2025**, 15 (3), 1443-1456, Article. DOI: 10.22052/JNS.2025.03.058 Scopus.
- 33. Ayalew, A.; Gonte, R. R.; Balasubramanian, K. <u>Development of polymer composite beads for dye adsorption</u>. *International Journal of Green Nanotechnology* **2012**, 4 (4), 440-454.
- 34. Bdaiwi, Z. M.; Ghanem, H. T. <u>Synthesis and characterization of some oxazepine compounds from 2- amino thiazole</u>. *Journal of Global Pharma Technology* **2020**, 12 (6), 291-303, Article. Scopus.
- 35. Saadallah K; AD C; Djedid M; Batool M; Benalia M; Saadallah S; Hamamda S. Potential of the Algerian pine tree bark for the adsorptive removal of methylene blue dye: Kinetics, isotherm and mechanism study. Journal of Dispersion Science and Technology. 2024:1-19
- 36. Radhy ND; Jasim LS. A novel economical friendly treatment approach: Composite hydrogels. Caspian Journal of Environmental Sciences. 2021;19(5):841-852.10.22124/cjes.2021.5233
- 37. Arumugam, T.; Krishnamoorthy, P.; Rajagopalan, N.; Nanthini, S.; Vasudevan, D. <u>Removal of malachite green from aqueous solutions using a modified chitosan composite.</u> *International journal of biological macromolecules* **2019**, 128, 655-664
- 38. Sun S; Bao D; Zhou Y; Cheng C; Zhang S; Zhao M; Guo J. Sodium alginate/chitosan-coated TiO2NPs hybrid fiber with photocatalytic self-cleaning property, UV resistance and enhanced tensile strength. International Journal of Biological Macromolecules. 2023;242:124966
- 39. Rashidzadeh B; Fathalipour S; Hosseini SP; Bazazi S. Alginate doped graphene oxide—TiO2—Fe3O4 nanocomposite: preparation, characterization, and application of sonophotocatalyst for efficient decomposition of an organic dye. International Journal of Environmental Analytical Chemistry. 2024;104(8):1911-1927
- 40. Salehi, R.; Arami, M.; Mahmoodi, N. M.; Bahrami, H.; Khorramfar, S. <u>Novel biocompatible composite (chitosan-zinc oxide nanoparticle): preparation, characterization and dye adsorption properties.</u> *Colloids and Surfaces B: Biointerfaces* **2010**, 80 (1), 86-93.
- 41. Hasanzadeh, M.; Simchi, A.; Far, H. S. <u>Nanoporous composites of activated carbon-metal organic frameworks for organic dye adsorption: Synthesis, adsorption mechanism and kinetics studies.</u> *Journal of Industrial and Engineering Chemistry* **2020**, 81, 405-414.
- 42. Oukebdane K; Necer IL; Didi M. Binary comparative study adsorption of anionic and cationic azo-dyes on Fe3O4-bentonite magnetic nanocomposite: kinetics, equilibrium, mechanism and thermodynamic study. Silicon. 2022;14(15):9555-9568